Journal Pre-proof

Modelling of killer T-cell and cancer cell subpopulation dynamics under immuno- and chemotherapies

Anni S. Halkola, Kalle Parvinen, Henna Kasanen, Satu Mustjoki, Tero Aittokallio

Please cite this article as: Anni S. Halkola, Kalle Parvinen, Henna Kasanen, Satu Mustjoki, Tero Aittokallio, Modelling of killer T-cell and cancer cell subpopulation dynamics under immuno- and chemotherapies, *Journal of Theoretical Biology* (2019), doi: https://doi.org/10.1016/j.jtbi.2019.110136

Highlights

- Model enables investigation of individualized effects of anti-PD1 immunotherapies

- Analysis of tumor burden, treatment times and T-cell loss by cytostatic treatments

- Model-based design of treatment schedules: initiation, duration and repetition

- Classes of patient trajectories including fixed steady states and cyclic attractors

- Combination of targeted and immunotherapy has better effect than mono-immunotherapy

Modelling of killer T-cell and cancer cell subpopulation dynamics under immuno- and chemotherapies

Anni S. Halkola[a,b], Kalle Parvinen[a,b,c], Henna Kasanen[d,e], Satu Mustjoki[d,e], Tero Aittokallio[a,b,f,*]

[a]*Department of Mathematics and Statistics, University of Turku, Turku, Finland*
[b]*Western Finland Cancer Centre (FICAN West), Turku University Hospital, Turku, Finland*
[c]*Evolution and Ecology Program, International Institute for Applied Systems Analysis (IIASA), Laxenburg, Austria*
[d]*Hematology Research Unit Helsinki, Department of Clinical Chemistry and Hematology, University of Helsinki and Helsinki University Hospital Comprehensive Cancer Center, Helsinki, Finland*
[e]*Translational Immunology Research Program, University of Helsinki, Helsinki, Finland*
[f]*Institute for Molecular Medicine Finland (FIMM), University of Helsinki, Helsinki, Finland*

Abstract

Each patient's cancer has a unique molecular makeup, often comprised of distinct cancer cell subpopulations. Improved understanding of dynamic processes between cancer cell populations is therefore critical for making treatment more effective and personalized. It has been shown that immunotherapy increases the survival of melanoma patients. However, there remain critical open questions, such as timing and duration of immunotherapy and its added benefits when combined with other types of treatments. We introduce a model for the dynamics of active killer T-cells and cancer cell subpopulations. Rather than defining the cancer cell populations based on their genetic makeup alone, we consider also other, non-genetic differences that make the cell populations either sensitive or resistant to a therapy. Using the model, we make predictions of possible outcomes of the various treatment strategies in virtual melanoma patients, providing hypotheses regarding therapeutic efficacy and side-effects. It is shown, for instance, that starting immunotherapy with a denser treatment schedule may enable changing to a sparser schedule later during the treatment. Furthermore, combination of targeted and immunotherapy results in a better treatment effect, compared to mono-immunotherapy, and a stable disease can be reached with a patient-tailored combination. These results offer better understanding of the competition between T-cells and cancer cells, toward personalized immunotherapy regimens.

Keywords: combination therapy, immunotherapy, personalized medicine, killer T-cells, side-effects

*Corresponding author. E-mail: teanai@utu.fi; Postal address: Vesilinnantie 5, 20500 Turku

1. Introduction

Each patient's cancer has a unique molecular makeup, often comprised of populations of genetically, functionally or epigenetically distinct cancer cell subpopulations that undergo dynamic evolutionary processes throughout the disease course and treatment periods. The goal of making cancer treatment more effective and personalized therefore requires an improved understanding of such dynamic processes, including evolutionary competition of space, glucose and other resources between cell populations that lead to the survival of fitter populations (Gillies et al., 2012; Glauche et al., 2018; Greaves, 2015). Mathematical modelling of heterogeneous cell population dynamics and treatment responses has shown great promise as a means to suggest mono- or combination therapies that can theoretically control or even inhibit distinct cancer cell populations, as well as provide mechanistic insights into treatment sensitivity and resistance for adaptive intervention designs (Bozic et al., 2013; Bozic and Nowak, 2014; Fischer et al., 2015; Louzoun et al., 2014; Michor and Beal, 2015; Zhang et al., 2017; Zhao et al., 2016). However, most of the modelling works have focused on genetic differences and architecture of sub-clones and their evolution, even though also non-genetic differences between or within tumors are known to contribute to the individual disease course and personalized responses to therapies in various hematological cancers and solid tumors, including patients with advanced malignant melanomas.

Melanoma is initiated by DNA mutations in melanocytes with major risk from exposure to ultraviolet light. Melanomas typically occurs in skin, where it forms lesions of irregular size, shape and color. In localized disease, common treatment is removal by surgery. However, in the case of advanced malignant melanoma where the disease has metastasized, multidisciplinary treatments, such as radiation therapy, targeted therapy (e.g., BRAF inhibitors such as vemurafinib), chemotherapy (e.g., dacarbazine) or immunotherapy (e.g., anti-PD-1 such as nivolumab and pembrolizumab) are recommended (Bhatia et al., 2009; Garbe et al., 2016; Maverakis et al., 2015). Novel immunotherapies have greatly improved the response rate, duration and tumor stability in patients with advanced melanoma even after treatment discontinuation (Huang et al., 2019; Topalian et al., 2014). However, varying treatment outcomes persist (Gauci et al., 2019), and despite the improved clinical benefit, a proportion of patients remain non-responsive leading to progressive disease (Robert et al., 2015). In some cases, the treatment has to be repeated periodically to control the cancer, leading to a chronic disease (Lipson et al., 2013). However, dormant cancer can also be reached (Aguirre-Ghiso, 2007; Ossowski and Aguirre-Ghiso, 2010; Schreiber et al., 2011; Senft and Ronai, 2016), where undetectable cancer persists after treatment.

Immune-checkpoint inhibitors are revolutionizing the treatment of patients with advanced-stage cancers. In particular, the blockade of programmed cell death protein 1 (PD-1) increases the survival of patients with metastatic melanoma and other solid tumors. Despite encouraging results, however, clinical outcomes of anti-PD-1 therapy remain highly variable and durable treatment benefit is limited to a minority of patients (Keenan et al., 2019). Immune-checkpoint inhibitors reactivate patient's immune system to defeat cancer, especially antigen-specific killer T-cells (or CD8+ T-cells). Approximately 20–50% of human cancers express programmed death-ligand (PD-L1) that inhibits the killer T-cell function by binding to its receptor PD-1 on the T-cell surface (Chen and Mellman, 2013). Monoclonal antibodies, such as anti-PD-1, block the inactivating binding of PD-L1 to its receptor protein PD-1 on killer T-cell surface, enabling the T-cell to attack the tumor (Pardoll, 2012) (see Supplementary Figure 1). Additionally, antigen delivery from dying cancer cells leads to increased activation of killer T-cells that elevates the regulation of T-cells also by other mechanisms, for example T-cell self-regulation. To understand the patient-specific responses to immunotherapies, one needs to take into account the dynamics and competition between active killer T-cells and cancer cells. Some of the currently unaddressed questions in melanoma therapy concern the timing of checkpoint blockage, respective benefits of targeted versus checkpoint inhibitors, and how to optimize the benefit-risk ratio of these regimens (Robert, 2018).

Immunotherapies are also being tested in combination with other cancer therapies, including targeted or cytotoxic chemotherapies, where the former inhibits the growth of cancer cells by interfering with specific

target molecules (e.g., oncogenes), whereas the latter prevents proliferation of the rapidly proliferating cells (e.g. traditional chemotherapy). The use of targeted treatments is preferred as they selectively kill cancer cells harboring a specific mutation or other molecular aberration that drives the particular cancer cell, and therefore they often cause less toxic effects in noncancerous cells. However, cancer cell populations without the aberration often remain resistant against the targeted treatment, and resistant subpopulations may also emerge by new mutations. For clinical applications, it is important to study the often subtle balance between the therapeutic efficacy and the degree of side-effects, especially when modelling the response of chemotherapies that lead to the death of both cancerous and T-cells. Even though heavy treatment dosage may potentially kill most cancer cells, the patient might not tolerate very intense treatment periods. There is a need to better understand various treatment choices and their scheduling, as those currently used in the clinics may not be optimal, but rather a result of trial and error or other considerations, such as cost issues.

In the present work, we introduce a comprehensive model for the dynamics of active killer T-cells and their competition against distinct cancer cell populations under various treatment modalities, including immunotherapies, targeted and chemotherapies. Rather than defining the cancer cell populations based on genetic differences alone, we consider cell populations that are either sensitive or resistant to a targeted therapy. Using the model, we make predictions of possible outcomes of the various treatment strategies and provide experimentally-testable hypotheses regarding, for example, therapeutic efficacy of treatment schedules (timing and duration) and toxic effects at different doses. As the first disease model, we chose melanoma, due to its clinical relevance and variety of options actually used in melanoma treatment. We demonstrate the behavior of the model dynamics in several case studies that model the effects of anti-PD-1 and targeted therapies, as well as their combinations, in comparison with chemotherapies in virtual melanoma patients characterized by key model parameters. Our modelling questions focus on the effects of therapy (particularly, targeted, chemo- and immunotherapy) on the cancer cell populations. In particular, how do patients respond to these treatments, when using different treatment initiation criteria (Case study 2), durations (Case studies 2, 3 and 4), dosages (Case study 4) or combinations (Case studies 3 and 4).

2. Materials and methods

2.1. Model overview

The dynamics of cancer cells and active killer T-cells are illustrated in Figure 1 for one cancer cell population (see Supplementary Figure 2 for multiple cancer subpopulations). Resources R correspond to nutrients, such as glucose, that flow in to and out of the microenvironment of cancer being modelled. Cancer cells (C) use these resources to divide. When a cancer cell dies, it delivers antigens, which then cause the activation of killer T-cells (T), leading to the increase in their number. The activated killer T-cells divide as well in the microenvironment. Each of the cell types undergo cell death caused either by apoptosis or drug treatments. T-cells have also self-regulation that is a way of the immune system to prevent overpopulation of killer T-cells.

The model parameters are listed in Table 1 and functions in Table 2. The cell-type specific proliferation strategy s_i is one of the key model parameters as it corresponds to the rate at which cancer cells consume resources to proliferate. The higher the strategy parameter, the more aggressive is the cancer subpopulation. Parameter γ specifies how much one resource unit contributes to cell division, assumed to be equal in all the cancer cell subpopulations.
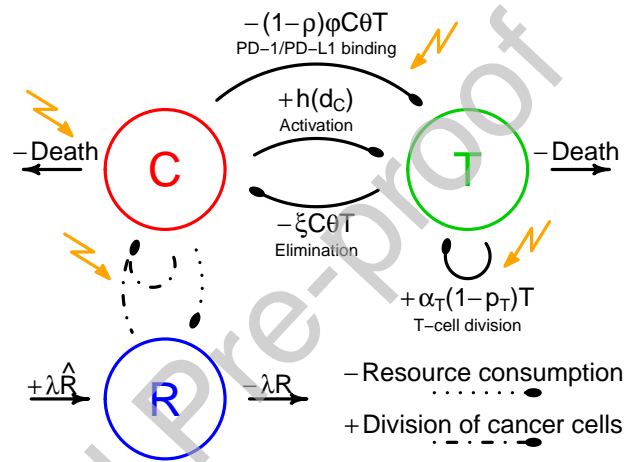
3

Figure 1: Presentation of the model as relations between different cell types (T for active killer T-cells, C for cancer cells) and resources (R). The other parameters are explained in Table 1. Positive terms increase the density and negative terms decrease the density with the ellipse pointing the affected entity. Cancer cell death includes both normal cell death and inhibition caused by targeted treatments and chemotherapies. T-cell death includes normal cell death, self-regulation and death caused by chemotherapy. Cancer cells consume resources to maintain their proliferative capacity. Killer T-cells get activated when they encounter cancer cells' antigens, but cancer cells can also inhibit T-cell activation by binding their ligands (such as PD-L1) to inhibitory receptors on T cell surface (such as PD-1). Lightning bolt arrows point the relations which are affected by different treatments. The extension of the model to multiple cancer cell subpopulations is presented in Supplementary Figure 2.

Symbol	Value	Unit	Meaning
$\hat{R}$	1.5	mass/volume	Concentration of resources flowing into the region of interest.
λ	1	-	Relative flow speed of resources.
$\boldsymbol{s_i}$	**varies**	-	The proliferation strategy of cancer cell subpopulation i.
α_0	0.1	$1/(\text{timeunit}*\#_C)$	Lower limit of $\alpha(\bar{s}_i)$.
a	1	$1/(\text{timeunit}*\#_C)$	Upper limit of $\alpha(s_i)$ is $\alpha_0 + a$.
b	0.5	-	The strategy value at which $\alpha(s_i) = \alpha_0 + a/2$
γ	0.8	$\#_C/(\text{mass/volume})$	Resource usage common to all cancer cells.
K	8	$\#_C$	The maximum amount of cancer cells in the region of interest.
μ_T	0.5	1/timeunit	Normal apoptosis rate of active killer T-cells.
μ_i	0.4	1/timeunit	Normal apoptosis rate of cancer cell subpopulation i.
w	0.7	-	Maximum proportion at which cancer cells limit each other's resource consumption.
$\boldsymbol{m}$	**varies**	$\#_T/\text{timeunit}$	Maximum rate of killer T-cell activation.
u	0.1	$\#/\text{timeunit}$	The amount of antigen delivery giving the half maximal activation.
v	2	-	The effect on the slope of $h(d_C)$ at u.
$\boldsymbol{\alpha_T}$	**varies**	$1/(\text{timeunit}*\#_T)$	Birth rate of active killer T-cells.
θ	0.6	-	Proportion of active killer T-cells that enter the region of interest.
ϵ	0.015	-	The proportion of delivered antigens by one normal cancer cell apoptosis, compared with death caused by drugs or killer T-cells.
$\boldsymbol{\xi_i}$	**varies**	$1/(\text{timeunit}*\#_T)$	Rate at which T-cells kill cancer cell subpopulation i.
$\boldsymbol{\varphi_i}$	**varies**	$1/(\text{timeunit}*\#_C)$	Rate at which cancer cell subpopulation i makes killer T-cells ineffective.
δ	0.6	$1/(\text{timeunit}*\#_T)$	Rate of active killer T-cell self-regulation.
$\boldsymbol{c(\tau)}$	**varies**	mass/volume	Concentration of a drug at time τ after adding the drug.

Table 1: Parameters of the model. Boldfaced parameters are changed in the case corresponding to cancer microenvironment of a virtual melanoma patient (see also Tables 2 and 3). $\#_T$ and $\#_C$ denotes density unit of T-cells and cancer cells as mass/volume and - denotes unitless variables.

5

Symbol	Equation	Unit	Meaning
$\alpha(s_i)$	eq. (4)	$1/(\text{timeunit}^*\#_C)$	Resource consumption rate specific for subpopulation i.
d_C	eq. (8)	$\#_C/\text{timeunit}$	The antigen delivery rate by dying cancer at time t.
$h(d_C)$	eq. (9)	$\#_T/\text{timeunit}$	Activation of killer T-cells.
H_p	eq. (10)	-	Hill equation expressing the effect of a cytostatic drug.
p_i	eq. (11)	-	Killing effect of cytostatic drug on cell type i
β_i	eq. (12)	$1/\text{timeunit}$	Killing effect of targeted drug on cell type i.
ρ_i	eq. (13)	-	Effect of immunotherapy.

Table 2: Functions of the model. $\#_T$ and $\#_C$ denotes density unit of T-cells and cancer cells as mass/volume; - denotes unitless variables

2.2. Model dynamics

We obtain the following ordinary differential equations (ODEs) for resources (R), cancer cell subpopulations (C_i) and active killer T-cells (T):

$$\frac{dR}{dt} = \lambda(\hat{R} - R) - \left(1 - w\frac{\sum\limits_j C_j}{1 + \sum\limits_j C_j}\right)\sum_j \alpha(\bar{s}_{C_j})RC_j \tag{1}$$

$$\frac{dC_i}{dt} = \gamma\alpha(\bar{s}_{C_i})\left(1 - w\frac{\sum\limits_j C_j}{1 + \sum\limits_j C_j}\right)RC_i\left((1 - p_i)\left(1 - \frac{\sum\limits_j C_j}{K}\right) - p_i\right) - \mu_i C_i - \beta_i C_i - \xi_i C_i \theta T \tag{2}$$

$$\frac{dT}{dt} = h(d_C) + (\alpha_T(1 - p_T) - \mu_T)T - \alpha_T p_T T - \frac{\delta}{2}T^2 - \sum_i(1 - \rho_i)\varphi_i C_i \theta T. \tag{3}$$

These ODEs are explained and justified in more detail in section 2.3. The Runge-Kutta method (RK45) was used to calculate numerically the dynamics of ODEs with R version 3.4.4 and RStudio version 1.1.453. Parameter values, especially the ones related to treatments, are altered to obtain multiple situations in the case studies corresponding to virtual melanoma patients characterized by combinations of model parameters. These virtual patient cases are presented in section 3.

2.3. Model details

This sub-section describes the model in more detail in the form of ODEs for resources R and each cancer cell subpopulation C_i in the microenvironment of cancer as well as for active killer T-cells T in the body. A resource-consumer model was used with logistic equation as the basis of competition between the cancer cell subpopulations.

2.3.1. Resources and cancer cells

Let R denote the concentration of resource (such as glucose) in the region of interest. Resources flow in and out following chemostat dynamics, that is, there is a constant inflow of medium with resource concentration $\hat{R}$, and the resource concentration of the outflowing medium equals R. The inflow and the outflow have the same flow speed λ, so that the volume of the resource medium in the region of interest remains constant. In

6

the absence of consumption, the resource concentration follows the differential equation $dR/dt = \lambda(\hat{R} - R)$ (Smith and Waltman, 1995).

When the cancer cell density is low, cancer cells consume resources according to the law of mass action (Tóth and Érdi, 1989), with the proliferation consumption rate $\alpha(s_i)$. It is assumed that this rate is of the form

$$\alpha(s_i) = \alpha_0 + a\frac{s_i/b}{1 + s_i/b}, \tag{4}$$

which is an increasing function of s_i with the upper limit of $\alpha_0 + a$. The upper limit is given since cells cannot consume resources infinitely fast. Even if cancer cells would lack division regulation, the cell cycle cannot happen infinitely fast. Additionally, high cancer cell density restricts resource consumption, for example, through increasing the distance between veins (Tannock, 1968). Therefore the resource consumption rate $\alpha(s_i)$ is multiplied by the factor

$$1 - w\frac{\sum\limits_{j} C_j}{1 + \sum\limits_{j} C_j}, \tag{5}$$

which is a decreasing function of the total cancer cell density and where w is the maximum proportion of restriction. The half saturation is reached when the total cancer cell density is one. However, with the chosen parameter values, the maximum total cancer cell density is around 0.8 in all case studies investigated in section 3 due to other restrictions, such as the amount of inflowing resources ($\hat{R}$), and thus the saturation $\sum\limits_{j} C_j/(1+\sum\limits_{j} C_j) < 0.5$.

The dynamics of cancer cells are determined by the balance between proliferation and apoptosis. It is assumed that cells attempt division with a rate that is directly proportional to their resource usage, with the conversion coefficient γ:

$$\gamma\alpha(s_{C_i})\left(1 - w\frac{\sum\limits_{j} C_j}{1 + \sum\limits_{j} C_j}\right)RC_i. \tag{6}$$

However, not all attempted divisions are successful. In the presence of a cytostatic drug, mitosis is interfered and the attempted cell division results in the death of the dividing cell with a probability p_i, which is further discussed in section 2.3.3. The division proceeds with the probability of $(1 - p_i)$. Furthermore, the microenvironment of cancer is assumed to have a carrying capacity, e.g., due to limitations of space, resulting in a variable likelihood of a successful division

$$1 - \frac{\sum\limits_{j} C_j}{K}, \tag{7}$$

which decreases with the total cancer cell density.

Cancer cells of type i have a natural death rate μ_i, and targeted drugs increase the death rate by β_i, depending on sensitivity or resistance of the cancer subpopulation to the drug. Modelling of the treatment effects are discussed in more detail in section 2.3.3. Additionally, active killer T-cells that enter the microenvironment of cancer (θT) kill cancer cells with the subpopulation-specific rates ξ_i. If a cancer cell subpopulation i does not present the antigen that T-cells are specific for, active killer T-cells do not recognize the cells at all ($\xi_i = 0$).

7

2.3.2. Active killer T-cells

When cancer cells face cell death, they deliver antigens to the blood stream (Chen and Mellman, 2013). The total rate at which such antigens are delivered is given by

$$d_C = \sum_i \left(\epsilon \mu_i + \gamma \alpha(\bar{s}_i) \left(1 - w \frac{\sum C_j}{1 + \sum C_j} \right) R p_i + \beta_i + \xi_i \theta T \right) C_i, \tag{8}$$

which includes normal cancer cell death (μ_i), death by drugs as well as death caused by active killer T-cells ($\xi_i \theta T$). Here, $\epsilon < 1$ specifies the proportion of delivered antigens by one normal cancer cell apoptosis (poorly immunogenic), compared with death caused by drugs or killer T-cells (immunogenic cell death) (Ferguson et al., 2011; Zhou et al., 2019). The delivery of antigens leads to the activation of antigen-specific killer T-cells from naïve T-cells, so that killer T-cells are produced with the rate

$$h(d_C) = m - \frac{m}{1 + (d_C/u)^v}, \tag{9}$$

which is an increasing function of antigen delivery rate d_C, where m is the maximum rate of killer T-cell activation and $h(u) = m/2$ and v affects the slope at u. Sigmoid function is chosen since small amount of antigen delivery might not be sufficient to invoke proper activation due to lack of a robust signal and complexity of immune response (Motz and Coukos, 2013). The amount of naïve T-cells is assumed to be large compared with the activation rate $h(d_C)$, so that the amount of naïve T-cells can be assumed to be constant and $h(d_C)$ is scaled accordingly.

Active killer T-cells proliferate with the rate α_T and they go through normal cell death at the rate μ_T. Since killer T-cells do divide, they are inhibited by cytostatic drugs with the rate p_T, leading to restricted proliferation and increased cell death, which are considered toxic side-effects. In contrast, targeted treatment is assumed not to affect T-cells directly but only trough increasing antigen delivery (8) by cancer cell death. Active killer T-cells circulate in the body until they detect their target and infiltrate into the tumor microenvironment (Chen and Mellman, 2013). The proportion of active killer T-cells present in the microenvironment of cancer is assumed to be constant θ for simplicity. These T-cells θT then proceed to kill cancer cells. However cancer cells use the PD-1/PD-L1 binding to make active killer T-cells ineffective, with the subpopulation-specific intensities φ_i. If a cancer subpopulation i does not have PD-L1, then $\varphi_i = 0$. The dynamics of the ineffective killer T-cells are not considered in the model. Immunotherapy, such as anti-PD-L1/anti-PD-1, is be used to prevent the binding of PD-1 and PD-L1 (Chen et al., 2012), and this happens with the cancer cell-type specific rate ρ_i, as further discussed in section 2.3.3. The immune system uses self-regulation to prevent overpopulation of killer T-cells and autoimmune disease (Disis, 2010), and this is modelled as T-cells interacting with each other with the rate δ.

2.3.3. Treatment modelling

The dose-response effect of a cytostatic drug with a concentration of $c_p(\tau)$ is modelled using the Hill equation (Gesztelyi et al., 2012):

$$H_p = H(c_p(\tau), IC50_p, n_p) = 1 - \frac{1}{1 + (c_p(\tau)/IC50_p)^{n_p}}, \tag{10}$$

where $IC50$ is the half-maximal inhibitory concentration and n, so called Hill coefficient (Gesztelyi et al., 2012), affects the slope of the Hill function at the concentration $IC50$.

The activity of chemotherapy is based on the proliferation rates of cells. For example, some nerve cells hardly divide, whereas most cancer cells divide rapidly, making them more vulnerable to the cytostatic drugs. However, there might be differences in the proliferation rates between cancer cell subpopulations within the same tumor. Chemotherapy disrupts cell division by damaging benchmarks in the cell cycle

(Malhotra and Perry, 2003). The more rapidly dividing cell populations reach those benchmarks more often, and therefore do not have time to repair, causing a cell death. Cytostatic drugs cause failure of division, followed by cell death, with the probability p_i, and so division proceeds with the probability $1 - p_i$, where

$$p_i = p(\bar{s}_i) = \frac{s_i}{1 + s_i} H(c_p(\tau), IC50_p, n_p) \tag{11}$$

with the subscript p denoting the Hill parameters of the cytostatic drug. In addition to the dose-response effect by Eq. (10), the probability p_i depends on the proliferation strategy s_i, since the speed of cell division affects the outcome of cytostatic treatment.

Molecularly-targeted treatments often have less side-effects, and therefore their clinical use is warranted provided one can select treatments targeting the patient-specific cancer driver mutations or other molecular targets. In case there are no effective drugs for a resistant cancer subpopulation, there is another way to control the resistant subpopulation by letting more rapidly dividing, sensitive cancer cells dominate the resistant ones. The sensitive cancer subpopulation is controlled by the treatment (Zhang et al., 2017). Targeted therapy increases death rate by β_i which follows the Hill equation (12). If the drug does not affect cell type i, the rate $\beta_i = 0$, otherwise

$$\beta_i = 1 - \frac{1}{1 + (c_\beta(\tau)/IC50_\beta)^{n_\beta}}, \tag{12}$$

where the subscript β denotes the Hill parameters for the targeted drug.

In this model, cancer cells use PD-1/PD-L1 binding to disturb the immune response, and hence anti-PD-L1/anti-PD-1 can be used as immunotherapy. Immunotherapy reduces PD-1/PD-L1 binding by the cancer cell subpopulation-specific intensity

$$\rho_i = \frac{(c_\rho(\tau)/EC50_\rho)^{n_\rho}}{1 + (c_\rho(\tau)/EC50_\rho)^{n_\rho}}, \tag{13}$$

where $EC50_\rho$ is the concentration that produces half-maximal efficacy and n_ρ affects the slope at $EC50_\rho$. When the drug concentration $c_\rho(\tau)$ gets bigger, ρ_i approaches 1. This is desired since $\rho_i = 1$ would mean complete prevention of unwanted PD-1/PD-L1 binding modelled by $(1 - \rho_i)C_i\theta T$.

The treatment is given as an infusion at the beginning of a treatment period, during which the drug concentration is assumed to be a positive constant for simplicity. After the treatment period the drug concentration is assumed to be zero. The length of the treatment period is varied to consider the differences in drug clearance in the case of infusion. If the treatment is given as daily dosages, it is done only during the treatment period that determines for how long the daily dosages are given without a break (drug holiday).

2.4. Measures

The following numeric measures are calculated from the model dynamics. They are used to quantify and compare different situations in terms of medical outcomes.

Treatment effect

The treatment effect is monitored by cancer cell population mean density, calculated as the integral of the amount of cancer cell population over time divided by the length of the selected time period. Additionally, the maximum of total cancer cell density ($C_{\max}$) quantifies the maximal tumor burden of the patient during the given time interval. In some cases, the total cancer cell density decreases after reaching the $C_{\max}$. However, even a transient high $C_{\max}$ may be fatal to the patient. The methods to measure of total cancer density or cancer burden depend on the cancer type. For melanoma and many other solid tumors, changes in tumor burden in the clinical evaluation of cancer therapeutics is typically measured with anatomical assessment of

tumor volume or area using imaging technologies (Dancey et al., 2008).

Side-effects

The side-effects are considered as the amount of T-cell loss caused by cytostatic drugs, which is calculated as the proportion of the amount of dead T-cells caused by cytostatic drugs to the overall loss of T-cells (death or changing to inefficient form because of PD-1/PD-L1 binding). The scaling is done so that levels of multiple situations can be compared with each other.

Time in treatment

Treatments cause also complications other than toxic effects on the patient, such as time spent in hospital, which results in variable tolerability. Additionally, more treatment cycles usually means more drugs, leading to higher costs of treatment. To take such burdens of treatment into consideration, we calculated the proportion of time in treatment by dividing the total period of time spent in treatment by the overall time interval.

3. Results

We demonstrate the model dynamics using several case studies that correspond to virtual melanoma patients characterized by key biological model parameters. We especially focus on modelling the personalized effects of immunotherapies, such as pembrolizumab or nivolumab, which are anti-PD-1 molecules with similar mode-of-action. In clinical practice, nivolumab is given to patients every 2nd week and pembrolizumab every 3rd week. However, the optimal timing and duration of these treatments is poorly understood either alone or in combination with other therapies, such as targeted therapies (e.g. BRAF or C-KIT inhibitors) or chemotherapies (e.g. dacarbazine or temozolomide). Therefore, our case studies are determined by changing personal model parameters that affect the dynamics of active killer T-cells and their competition against cancer cell subpopulations, for example cancer cells' effectiveness against killer T-cells (φ_i) or maximum activation of killer T-cells (m) in an individual patient. Those parameters that are changed in the case studies are marked with bold font in Table 1, and their values are listed in Table 3. Each case is started with cell densities of 0.05 for all cell types.

The majority of parameter values were obtained by testing if numerical solutions are reasonable in comparison to the observed clinical outcomes in melanoma and other solid tumors (Aguirre-Ghiso, 2007; Ossowski and Aguirre-Ghiso, 2010; Schreiber et al., 2011; Senft and Ronai, 2016; Topalian et al., 2014; Wolner et al., 2018). Additionally, sensitivity analysis of the model parameters was performed to identify those parameters having highest effect on the numerical solutions (see section 3.6 and Supplementary section 8). The doubling times were calculated for melanoma cells in each case study as explained in Supplementary section 3. The doubling times were reasonable compared to experimental results in melanoma cells (Laing et al., 2003). Killer T-cell parameters were chosen so that small density is reached in the absence of cancer cells if initial T-cell value is positive (some T-cells remain in the system after defeating cancer). Additionally, the maximum rate at which cancer cells limit each other's resource consumption (w) multiplied by the saturation of cancer cells (maximum around 0.44) was compared to observations of 4–56% relative volume of necrotic tissue in melanoma (Tufto and Rofstad, 1998).

As different cancer types share similar qualities, some of the parameters are more generally related to cell functionality ($\hat{R}$, λ, γ, w and ϵ), while others are specifically linked to cancer type, here melanoma ($\alpha(s_i)$, μ_i, θ, ξ_i and φ_i). Parameters related to T-cell dynamics (α_T, μ_T, m, u, v and δ) do not specifically concern only killer T-cells working against melanoma. Treatment parameters ($c(\tau)$ and Hill-parameters) are specific to a drug and its effect on specific cancer type. Here the drug concentration is assumed constant during the treatment period, therefore also the effect (p_i, β_i or ρ_i) is constant. In addition to cancer specificity, some parameters are also considered patient specific as individuals have different melanoma subtypes and different physiology. Ideally, all parameters should be estimated individually, but in clinical practice

		Unit	Fig.2a	Fig.2b	Fig.2c	Fig.3	Fig.7	Fig.8
Parameter	s_{C_1}	-	1	1	1	1	1	1
	s_{C_2}	-	0.95	0.95	0.95	-	0.95	0.95
	α_T	$1/(\text{timeunit}*\#_T)$	0.505	0.505	0.267	0.505	0.505	0.505
	$\xi_{1,2}$	$1/(\text{timeunit}*\#_T)$	1.5	1.5	1.5	1.5	2	1.5
	$\varphi_{1,2}$	$1/(\text{timeunit}*\#_C)$	5	1	1	3	4	3
	m	$\#_T/\text{timeunit}$	0.5	0.5	1.5	0.5	0.5	0.5
Treatment	$\rho_{1,2}$	-	0.999	-	-	0.999	0.999	0.999
	β_1	$1/\text{timeunit}$	-	-	-	-	0	-
	β_2	$1/\text{timeunit}$	-	-	-	-	0.432	-
	$c_p(\tau)$	mass/volume	-	-	-	-	-	$0.5-5$
	$IC50_p$	mass/volume	-	-	-	-	-	2
	n_p	-	-	-	-	-	-	2
	Cancer doubling time in days		8	7	6	6	8	8

Table 3: Parameters and their values that vary between case studies. Cancer doubling time presents the doubling time of cancer cells in total when no treatment is used (calculations in Supplementary section 3). Calculated doubling times are close to median potential doubling time for melanoma cells of 8.6 days reported in experimental studies (Laing et al., 2003).

this is still impossible and generally estimated values have to be used. However, most important parameters that should be estimated individually are parameters that relate to the interactions between cancer cells and T-cells (ξ_i and φ_i). Additionally, the infiltration of T-cells (θ) varies as some cancers modify the environment to block the T-cell infiltration, and cancer cells might even inhibit the development of immune response in the first place ($m = 0$)(Chen and Mellman, 2013).

In the case studies, maximum of two cancer cell subpopulations were included for simplicity (denoted by C_1 and C_2) to demonstrate the model behavior when one subpopulation divides faster than the other ($s_{C_1} > s_{C_2}$). Additionally in the third case study (section 3.4), where targeted therapy is used, one subpopulation was considered resistant ($\beta_1 = 0$) and the other sensitive ($\beta_2 > 0$) to the targeted treatment. There could be also other differences between the cancer cell subpopulations, for example, one subpopulation might not present the same antigen causing ineffectiveness of T-cells ($\xi_i = 0$). However, these possibilities are not investigated here due to increased complexity. In the case studies, the concentration of targeted therapy and immunotherapy are kept constant, hence for β_i and ρ_i only the effect size is given instead of concentration.

3.1. Baseline cases: no treatment

We first investigated selected patient cases without any treatment (i.e. baseline cases). In some cases this means that cancer cells will eventually dominate, resulting in a decreased amount of active (and effective) killer T-cells in the body. Interestingly, changing the behavior of killer T-cells relative to that of cancer cells may also lead to cases where killer T-cells are able to control cancer cells even without treatment. Some representative cases are presented in Figure 2, where the cell densities of the model are shown as a function of time.

Figure 2a presents a challenging case, where the amount of active killer T-cells decreases monotonically and the total amount of cancer cells increases to a maximum level. Notably, after around 40 days, the
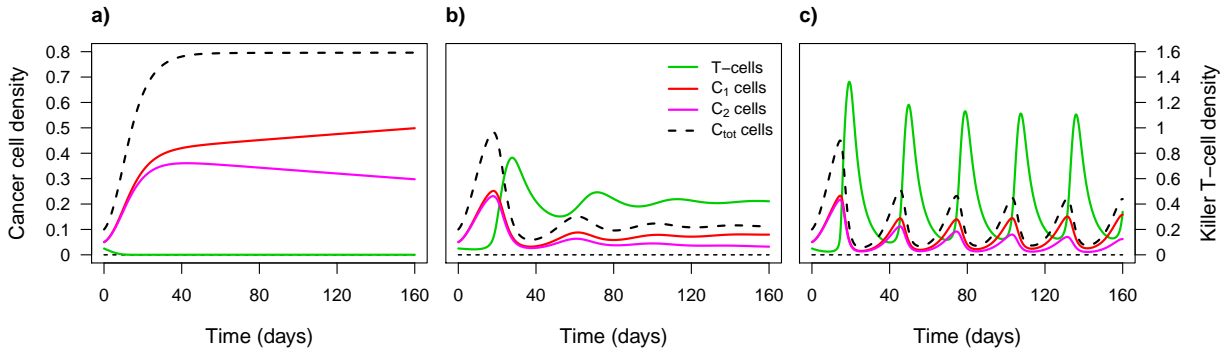
Figure 2: Three representative cases of dynamic competition between active killer T-cell (T) and cancer cell populations (C_1 and C_2) at baseline (no treatment). Here one subpopulation (C_1) divides faster and eventually dominates the less aggressive subpopulation (C_2). The differences between subpopulations affect, for example, the treatment outcome, when the different cancer cell subpopulations (here C_1 and C_2) also have other undesirable qualities (e.g., treatment resistance, metastatic capabilities or promotion of angiogenesis). In real patient case, for example, formation of metastases would be more likely if the faster dividing subpopulation also has elevated metastatic capabilities. a) Active killer T-cells decrease without treatment, leading to fast increase of cancer cells toward a maximum level (here, 0.80). The maximum amount of cancer cells is restricted by carrying capacity of the cancer microenvironment as well as by the sufficiency of resources. This baseline case is further investigated when treatment is given in section 3.3. b) The amount of active killer T-cells increases without treatment, leading to decreased amount of cancer cells. The cancer cell amounts alternate, but they are approaching a fixed steady state, which reflects the case when the initial immune response is effective and cancer is not even detected. c) Whenever the amount of cancer cells try to increase, the active killer T-cells increase accordingly, but decreases steeply after cancer cell count has decreased. In this case, the density of killer T-cells and cancer cells approach a cyclic attractor that defines their balance in the absence of treatment or other intervention. All parameter values are listed in Tables 1 and 3. Trajectories of b) and c) are presented in Supplementary Figure 4.

cancer cell subpopulation C_2 also starts decreasing, since the other cancer subpopulation C_1 proliferates more aggressively, and therefore starts to dominate also C_2. In this case, treatment is needed, and different treatment options are further discussed in section 3.3.

Figure 2b presents a positive case, where active killer T-cells are more effective against cancer cells, whereas cancer cells' PD-1/PD-L1 binding is expressed less than in Figure 2a. This results in a situation where active killer T-cells manage to control the cancer cells without treatment, and their amounts fluctuate and approach a fixed steady state (stable attractor). If the active killer T-cells proliferate less often, while the T-cell activation is increased, the active killer T-cells defeat cancer cells in each relapse attempt, resulting in a cyclic attractor (Figure 2c). Periodic behavior has been found both in cancer (Fortin and Mackey, 1999) and in the immune system (Stark et al., 2007) so likely it is possible also in the competition between immune system and cancer cells. However, such cyclic behavior presents a phenomenon that is likely to take place in the very early phases of the disease, when immune system is still able to control the growing tumor (Dunn et al., 2004; O'Donnell et al., 2019). Thus the melanoma might not yet be diagnosed and treated and cyclic behavior may well have gone undetected so far in real patient cases and clinical trials.

These representative cases demonstrate how different values in the key model parameters related to underlying biology result in both inter-patient and intra-tumor variation in disease progression, and influence the individual physiology and pathophysiology. In some cases, the immune system deals with the cancer progression so early the cancer might not even be detected and diagnosed. However, some patients do need treatment, and how to tailor it to the individual needs is investigated in the following sections.

12

3.2. Case study 1 - single-shot immunotherapy

In the first case study we investigate the effect of immunotherapy on the virtual melanoma patient presented in Supplementary Figure 5a without treatment. The dynamics without treatment are similar to Figure 2a, however only one cancer cell subpopulation is considered in order to investigate the attractor landscape more easily. To start treating the patient, an anti-PD-1 immunotherapy is given when the total amount of cancer cells exceeds a pre-defined threshold (here, 0.5, a detection limit of a diagnostic test). Figure 3a shows the case of this patient with one treatment period starting at day 18 (gray bar). One treatment period of 16 days is already enough in this case to increase the amount of active killer T-cells to a level that suffices to control the cancer cells below the threshold. Such a dormant cancer has been also reported in real patients (Aguirre-Ghiso, 2007; Ossowski and Aguirre-Ghiso, 2010; Schreiber et al., 2011; Senft and Ronai, 2016). Additionally, major pathologic responses after a single dose of anti-PD-1 were observed also in real patients (Huang et al., 2019; Tokuyasu et al., 2019).

From Figure 3a it can be seen that both the killer T-cells and cancer cells start to approach a fixed steady state that is different from the steady state reached without treatment. To illustrate dynamics near the different attractors, we constructed phase plane diagrams (Figures 3b and 3c). The two phase plane diagrams show how the given treatment causes a change in the isoclines and the steady state changes from the red circle in Figure 3b to the intersection of black lines in Figure 3c. During treatment the trajectory starts to reach the new attractor (solid blue line in Figure 3c). Once the treatment is stopped, the phase plane and attractors return to that of Figure 3b and the cell densities are located on the phase plane in such relation to attractors that the original attractor is unattainable; instead, a better situation for the patient, with decreased cancer cell density and increased killer T-cell density, is reached. With insufficient treatment (too short duration or too small dosage), the cell population dynamics end up to the original attractor, corresponding to no treatment (red circle).

This case study demonstrates how there may exist multiple attractors, and the ones with smaller density of cancer cells could be considered as more favorable for the patient. It is also evident that differently behaving cells (e.g., more aggressive cancer cells or less effective killer T-cells) result in different phase planes and attractor landscapes. Some steady states could be reached with only one sufficient treatment period, whereas cyclic attractors are observed when repeated treatments are required, both indicating stable diseases that are under control with the proper treatment. An absence of an asymptotic trajectory (either fixed or cyclic) indicates a progressive disease. In the following sections, the virtual patient cells harbor more than one cancer population, which cause more complex phase planes and model behavior.

3.3. Case study 2 - repeated immunotherapy

Let us next consider another virtual patient, with such aggressive cancer, consisting of two subpopulations, that cannot be stabilized with single treatment period alone, but who requires repeated immunotherapy. At baseline, without any treatment, the cell population densities of this patient are as in Figure 2a. Therapy is clearly needed, and it is considered to be given using two different regimens, either pre-defined or adaptive treatment initiation, which are compared in the following subsections.

3.3.1. Pre-set treatment periods versus threshold-based treatment initiation

A widely-used treatment option is to pre-set treatment periods with pre-set intervals (e.g. Figure 4a). The duration of treatment period and the intervals between treatments (so-called drug holiday) are changed to illustrate different schedule options for pre-set periods. It is observed from the mean density of total cancer cells, as expected, that shorter treatment durations require shorter drug holidays for an effective treatment outcome (Figure 4c). The corresponding mean densities of the killer T-cells (Figure 4e) give similar results as T-cell level does not increase if the drug holiday is too long compared to the treatment period.
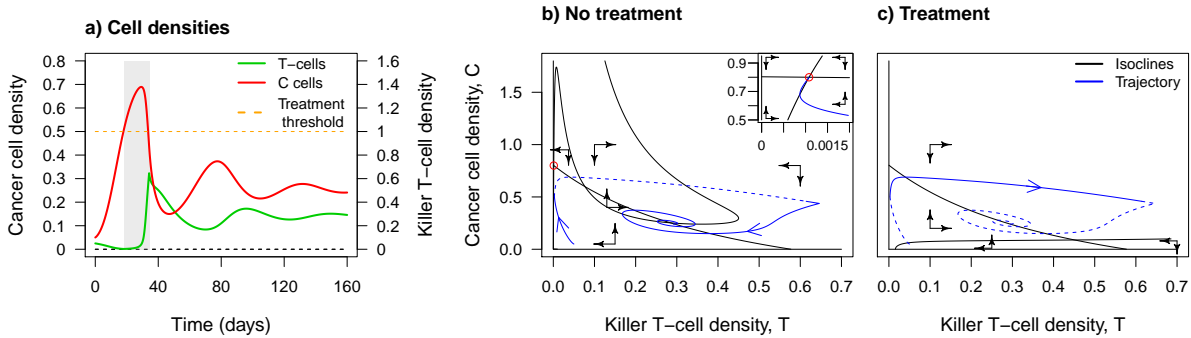
13

Figure 3: Single-shot immunotherapy. a) Immunotherapy is given for a period of 16 days (grey bar), started when the total amount of cancer cells exceeds a threshold of 0.5 (dashed orange line). During the treatment, the drug concentration is assumed constant resulting in a constant treatment effect. In this case, the treatment almost completely prevents PD-1/PD-L1 binding and thus prevents cancer cells from making active killer T-cells ineffective ($\rho_i \approx 1$). b) and c) Phase plane plots showing the isoclines (black lines) of the killer T-cell density T and cancer cell density C, b) during no treatment and c) during treatment. It is assumed that dynamics of resources are fast and in their stable state at each point. The trajectories shown with respect to time in panel a) are shown also in the phase plane plots (blue lines). The trajectory is plotted with a solid curve when the actual treatment status is the same as in the phase plane plot (treatment or no treatment). Red circle marks the fixed attractor that would have been reached without treatment and this area is zoomed on the top right corner with blue line denoting the trajectory when no treatment is used. c) The corresponding phase plane when immunotherapy is used. Solid blue line corresponds to the trajectory during treatment while dashed blue line is the trajectory when no treatment is used.

Another, more adaptive option is to start treatment only when the total cancer cell count (i.e., total tumor burden) exceeds a given threshold, and then treat for a pre-set period until the total tumor burden goes below the threshold (e.g. Figure 4b). One interesting observation is that a selected treatment threshold gives quite similar mean densities (Figures 4d and 4f) regardless of the treatment period, because shorter treatment periods are repeated if the cancer cell count remains still over the threshold. As expected, the mean density of total cancer cells increases when the threshold is increased since higher cancer levels are allowed before the treatment is started.

A practical question is: which of these options, pre-set periods or threshold-based treatment initiation, should be chosen for a given patient? Perhaps not surprisingly, the answer depends on the parameters of the treatment regimen: the duration of the treatment period, relative to the intervals between treatments, and the chosen threshold level. By choosing specific combinations, either one of the two regimens can result in a smaller mean density, and hence better therapeutic effect. To give an example, where pre-set periods results in a smaller total cancer mean density when equally long treatment periods are chosen, red boxes are marked in Figure 4c (pre-set periods) and in Figure 4d (threshold). On the other hand, choosing of treatment combinations of the blue boxes of Figures 4c and 4d results in smaller mean density for the threshold-based regimen. These four cases are shown separately in Supplementary Figure 6.

Considering only the mean density as a measure of treatment benefit does not however give the whole truth, since it does not take into account the overall time of treatment for the various regimens. For example, choosing a long treatment period with short gaps between repeats means that treatment is almost continuous. Small treatment threshold value might also result in nearly continuous treatment. It can be seen from Figure 5, that the pre-set period has to be chosen carefully in order to reach beneficial results (a population mean close to 0.8 means that the treatment fails). On the other hand, successful treatment result can be reached also without increasing the time in treatment (in the chosen time interval), provided the relative timing of treatment period and drug holiday is chosen based on the individual characteristics (blue dotted line). When threshold-based treatment initiation is used, the shorter treatment periods are repeated if necessary and this leads to equal levels of overall treatment time (Figure 5 green symbols).

14

Overall, using a threshold-based adaptive regimen results in a successful treatment outcome (cancer is kept in control) more often, compared to pre-set periods, since the treatment is given as long as needed, although it might mean longer continuous treatment periods due to repeated periods. Drug holidays between the treatments, if too long, can easily cause a relapse that short treatment periods cannot overcome. In practice it is difficult to determine the amount of cancer at each time point, especially if the cancer is inside the tissues, therefore choosing the threshold-based treatment initiation might not be applicable unless diagnostic tests are improved.

3.3.2. Changing pre-set period of immunotherapy

The previous section demonstrated that if the pre-set treatment periods are applied with too long gaps between treatments, the treatment easily fails (i.e., cancer is not under control). On the other hand, it would be preferred to apply treatment as seldom as possible to reduce side-effects and costs of treatment. To investigate this trade-off, we next consider changing the pre-set treatment period after starting the immunotherapy to test the effect of having longer drug holiday between treatments. In Figure 6a, the treatment schedule is changed successfully after three treatment periods (48 days), which enabled increased drug holiday from 6 days to 16 days. Interestingly, whereas having such longer drug holiday from the beginning would result in a rapid treatment failure (Figures 4c and 6, and Supplementary Figure 6), starting with a tighter schedule makes it later possible to increase the treatment gaps, provided those are chosen based on patient characteristics. For instance, in Figure 6b, the new drug holiday is only slightly longer (20 days vs. 16 days), yet there is a marked increase in total cancer cell density due to longer drug holidays, during which the amount of killer T-cells decreases to a level from where the amount cannot recover any more, at least by the given treatment of 12 days. In Figure 6c, the treatment schedule is changed later (after 102 days), but this also leads to a treatment failure in this patient case, indicating that scheduling of the first treatment periods is critical for determining whether or not the treatment could be given with longer drug holidays later.

As the treatment starts to fail when going from the case of Figure 6a to 6b and 6c, it is not surprising that the cancer cell maximum and mean density increase, as well as the tumor burden after one year (barplots on the right-hand side of Figure 6). On the other hand, the proportion of time in treatment is longer in the case of Figure 6a than in the case of Figure 6b, since the treatment is given more often (the barplots below the dynamics). When comparing the treatment response of Figure 6a to that of Figure 4a (measures marked with blue lines on Figure 6) it is noticeable that the proportion of time in treatment is smaller (due to a sparser treatment schedule), but still resulting in similar cancer total density after one year. With the heaviest treatment schedule of Figure 4a (12 days treatment, 6 days drug holiday), the lowest mean population density is reached, as expected, but this comes at the expense of time spend in treatment. The practical question is: which one is more important for the patient. If the treatments are not well-tolerated, then it might be preferred to reduce the time in treatment, even if the tumor burden stays on a slightly higher level.

3.4. Case study 3 - combination of targeted and immunotherapy

In the previous sections, we investigated the virtual patients' responses to various regimens of immunotherapy only. In some cases, however, it might be more beneficial to combine the immunotherapy with targeted treatments, especially if it can be targeted to the patient's molecular aberrations, and in this way boost the treatment responses. To make the situation more challenging, we assume that the targeted treatment is effective against only one of the cancer cell subpopulations (C_2 in this case), whereas the other subpopulation is resistant to the targeted treatment.

To study the potential benefits of such personalized immune-treatments, we treated the virtual patient with various strategies, where the patient either receives immunotherapy alone (Figure 7a), which resulted
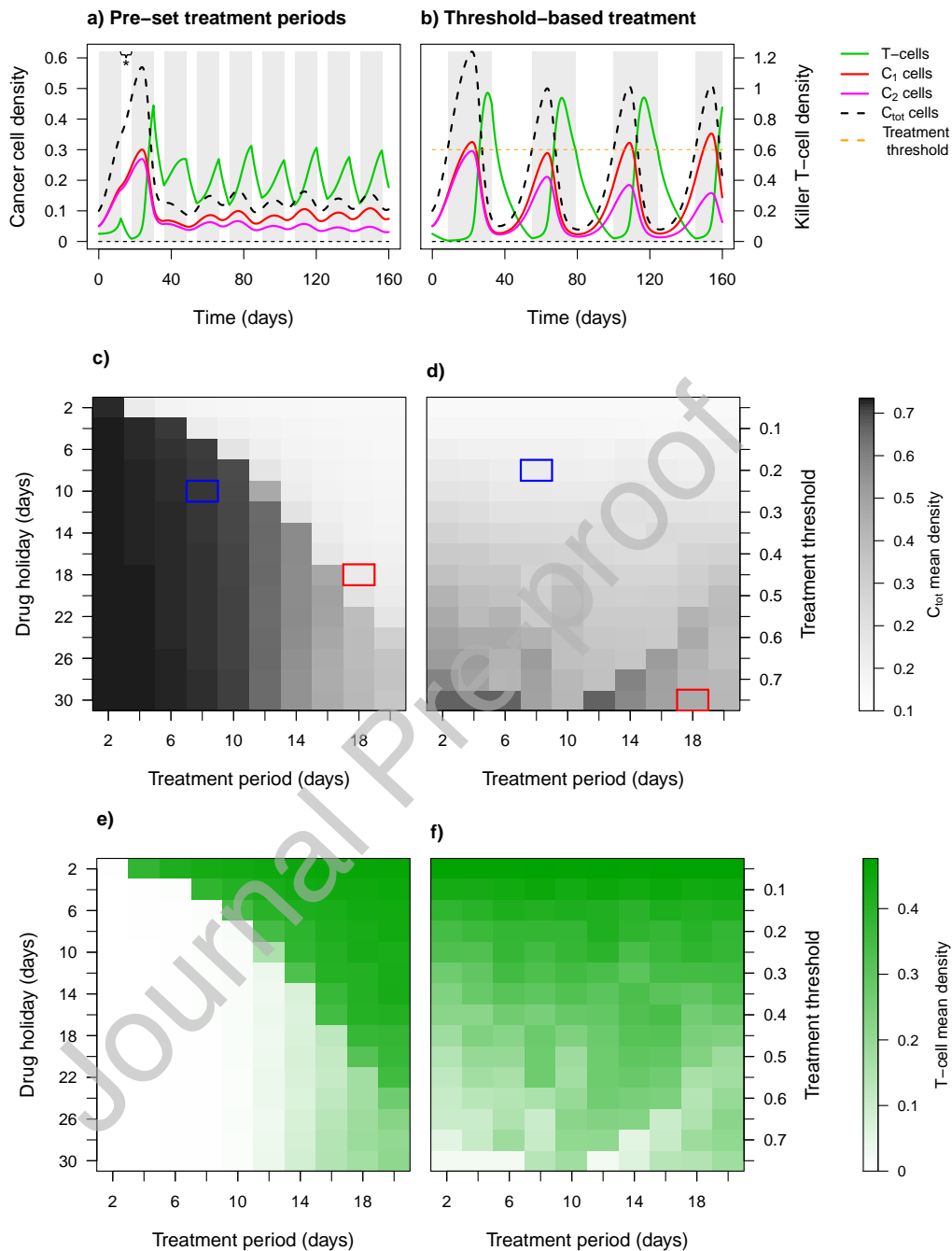
15

Figure 4: Pre-set immunotherapy periods versus threshold-based treatment initiation. a) Pre-set period of 12 days of treatment followed by 6 days of drug holiday. b) Immunotherapy is started when the total cancer cell density goes above the treatment threshold of 0.3, followed by 12 days period. Treatment is repeated at first three times and later two times since the cancer cell density stays over the threshold. c) Mean density of total cancer cells for different treatment periods and drug holidays (marked with * in panel a)). To give comparative examples, a few treatment options are marked with red or blue boxes. The red box corresponds to treatment period of 18 days, followed by a drug holiday of 18 days, with a mean population density of 0.20. In the blue box, the corresponding values are 8, 10 and 0.70. d) Mean density of total cancer cells for different treatment periods and thresholds of treatment initiation. The red box corresponds to treatment period of 18 days and threshold of 0.75, with a mean density of 0.49. In the blue box, the corresponding values are 8, 0.2 and 0.19. e) Mean population density of active killer T-cells in the case of pre-set treatment period, and f) in the case of threshold-based regimen.
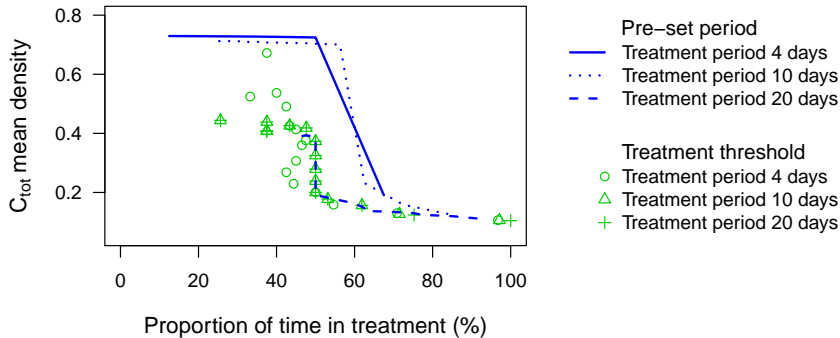
16

Figure 5: Mean population density of cancer cells drawn against the proportion of time in immunotherapy with selected treatment periods (4, 10 or 20 days), when using either pre-set periods or threshold. In the case of pre-set periods, the proportion of time in treatment depends on the period between treatments (drug holidays). In the case of threshold-based treatment initiation, treatment time depends on the used threshold level.

in a chronic disease with repeated treatment, or using a combination of targeted and immunotherapy (Figures 7b and 7c). Both of the treatments were initiated simultaneously, for simplicity, but their durations differ so that the combined treatment duration is always set to 14 days and its division to the two treatment options is varied. When both of the treatments have the same duration of 7 days (Figure 7b), the treatment has to be repeated, due to rapid decrease in the amount of killer T-cells, and eventually only the resistant cancer subpopulation C_1 stays alive, and the targeted treatment becomes useless. In contrast, when changing the durations of the treatment periods, it is possible to come up with more effective modalities in which the chosen drug combination leads to a situation where no further treatment is needed in order to keep the cancer density below the treatment threshold of 0.5 (Figure 7c). This is because after the second treatment period, the densities of cancer cells and killer T-cells trajectories reach a suitable balance that leads to a better attractor for the patient (in similar fashion as in section 3.2).

To investigate these situations more systematically, the total cancer mean densities are calculated when the treatment threshold is varied with the proportion of targeted treatment (Figure 7d). Additionally, to investigate the trade-off between therapy effect and therapy intensity, the corresponding numbers of treatment initiation are calculated (Figure 7e). One can see that with most treatment proportion combinations, smaller threshold leads to smaller cancer mean densities, but that also requires more treatment periods. Immunotherapy works by itself (0% of targeted therapy) but adding a small proportion of targeted therapy decreases total cancer cell mean density, while with most of the treatment thresholds, equal number of treatment initiations is needed.

Our model also predicts in this case study that combination therapy works better than targeted therapy alone. When only targeted treatment is used , if treatment is initiated too early (threshold ≤ 0.1), total cancer cell density increases rapidly to maximum value due to the targeted treatment being effective only on one cancer subpopulation, which decreases rapidly and only the resistant subpopulation remains. Since there is not enough sensitive cancer cells to deliver antigens in the first place, the density of T-cells does not increase sufficiently to dominate the resistant cancer subpopulation (C_1). However, if the treatment is initiated too late (threshold ≥ 0.31), the treatment succeeds once, followed by relapse, since by the time of the second treatment initiation, the density of the sensitive cancer subpopulation (C_2) has fallen too low, and the targeted therapy does not have enough effect to increase the level of killer T-cells.

Interestingly, if the treatment threshold is around 0.15–0.3 in this case, the targeted treatment is effec-
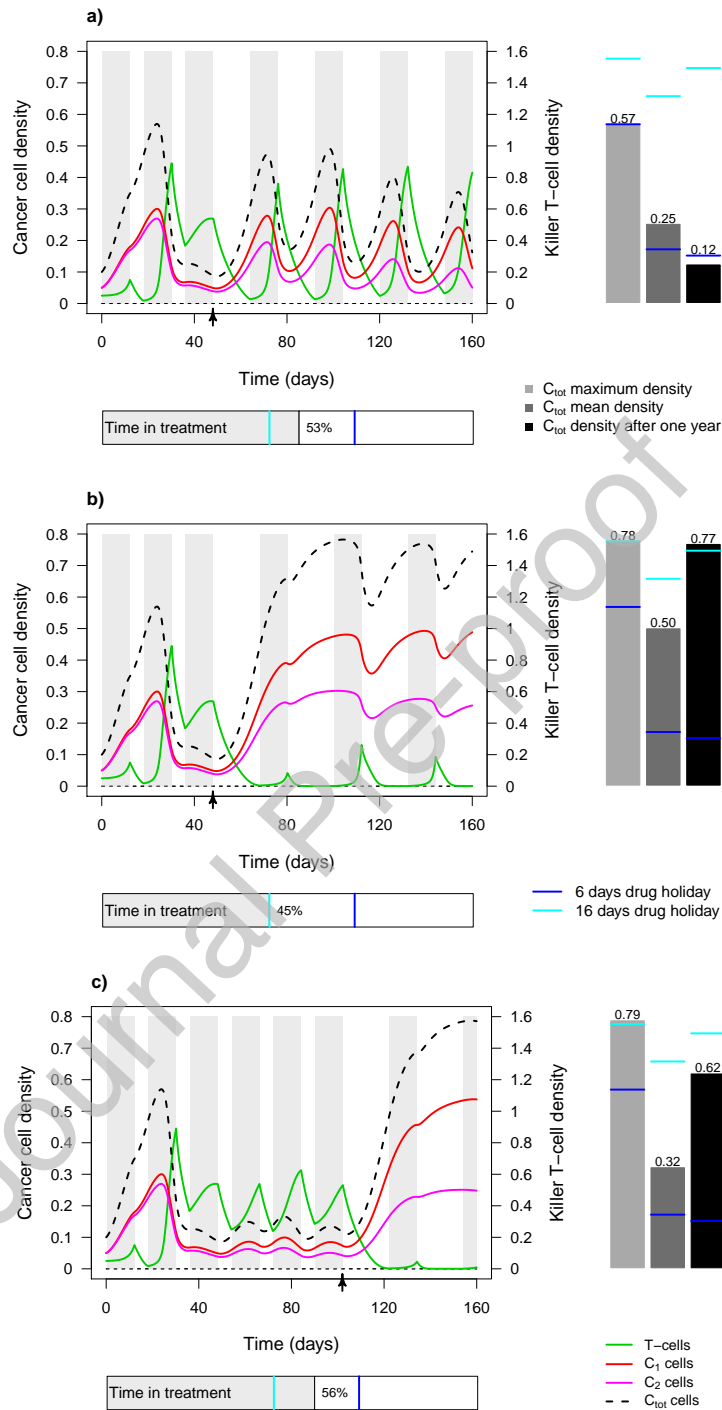
17

Figure 6: The effect of changing pre-set immunotherapy schedules. The treatment is started with a period of 12 days of treatment, followed by 6 days of drug holiday, which corresponds to Figure 4a. After 48 days (black arrow) treatment schedule is changed to have a drug holiday of a) 16 days or b) 20 days. c) Treatment schedule is changed after 102 days (black arrow), to have a drug holiday of 20 days. Right-side barplots: the treatment success measures are presented for each example, with blue lines marking the corresponding values for the case of Figure 4a, where treatment is continued with shorter drug holidays of 6 days. Cyan lines mark the case, where the treatment is started with 16 days of drug holiday from the beginning. Bottom bars: proportion of time spend in treatment.

tive also on its own without immunotherapy (when considering the total time interval of 160 days). For well selected treatment thresholds (e.g., 0.3) only four treatment initiations are needed, leading to similar stable disease as in Figure 7c. This surprising result is due to such optimal treatment initiation and period for this patient case that drive the cancer cell densities on the attractor landscape in a region which leads to a fixed steady state after the treatment. It should be noted that even though the combination treatment might result in some cases in a smaller tumor burden (cancer cell mean density), it may not be still beneficial from the treatment tolerability (and cost) point of view, when considering the total amount of drugs used, since each treatment period includes two (expensive) drugs instead of one. In an optimal and cost-effective therapy regimen, the amount of treatments needed should be minimized to compensate for the costs, along with possible tolerability issues caused by adding more treatments.

3.5. Case study 4 - combination of chemotherapy and immunotherapy

In the final case study, we consider a situation where a virtual patient does not have any targeted therapies matching to his/her cancer aberrations (C_1 or C_2) and who, without treatment, would have rapid increase in the total cancer cell density (Supplementary Figure 5c). Therefore, chemotherapy is the only option, used either alone (e.g. Figure 8a) or in combination with immunotherapy (e.g. Figure 8b). Since cytostatic drugs cause side-effects, their minimal use is preferred with small concentrations.

When changing the treatment period and concentration of the cytostatic drug, the proportion of time in treatment decreased in almost every case, when comparing the combination treatment to chemotherapy alone (Figure 8c, green shapes appear on the left side of the corresponding blue shapes). This indicates that adding the immunotherapy decreases the treatment time with additional possibility of smaller cancer cell mean density (Figure 8c, green shapes appear below or on similar level to the corresponding blue shapes).

The side-effects in this case are calculated as the proportion of T-cell loss caused by cytostatic drug to the overall T-cell loss, and they are investigated along with therapeutic effect (total cancer cell mean density) in Figure 8d across various treatment periods. When the combination of chemotherapy and immunotherapy is used and the treatment period is short (4 days), the side-effects are less than the side-effects caused by chemotherapy alone. However, when the treatment period is increased (20 days) the combination therapy causes slightly more side-effects than mono-chemotherapy, because the longer period of immunotherapy decreases more the overall loss of T-cells by preventing the PD-1/PD-L1 binding, and hence the proportion of T-cell loss caused by cytostatic drug increases.

The combination therapy leads to smaller or similar cancer population mean densities compared to chemotherapy alone, but the differences are not so dramatic that it would be clear which treatment regimen to choose only by looking at the cancer cell mean density or proportion of T-cell loss caused by chemotherapy. Additional considerations in practice involve the trade-off between the use of two treatments simultaneously or potential treatment tolerability issues caused by immunotherapy.
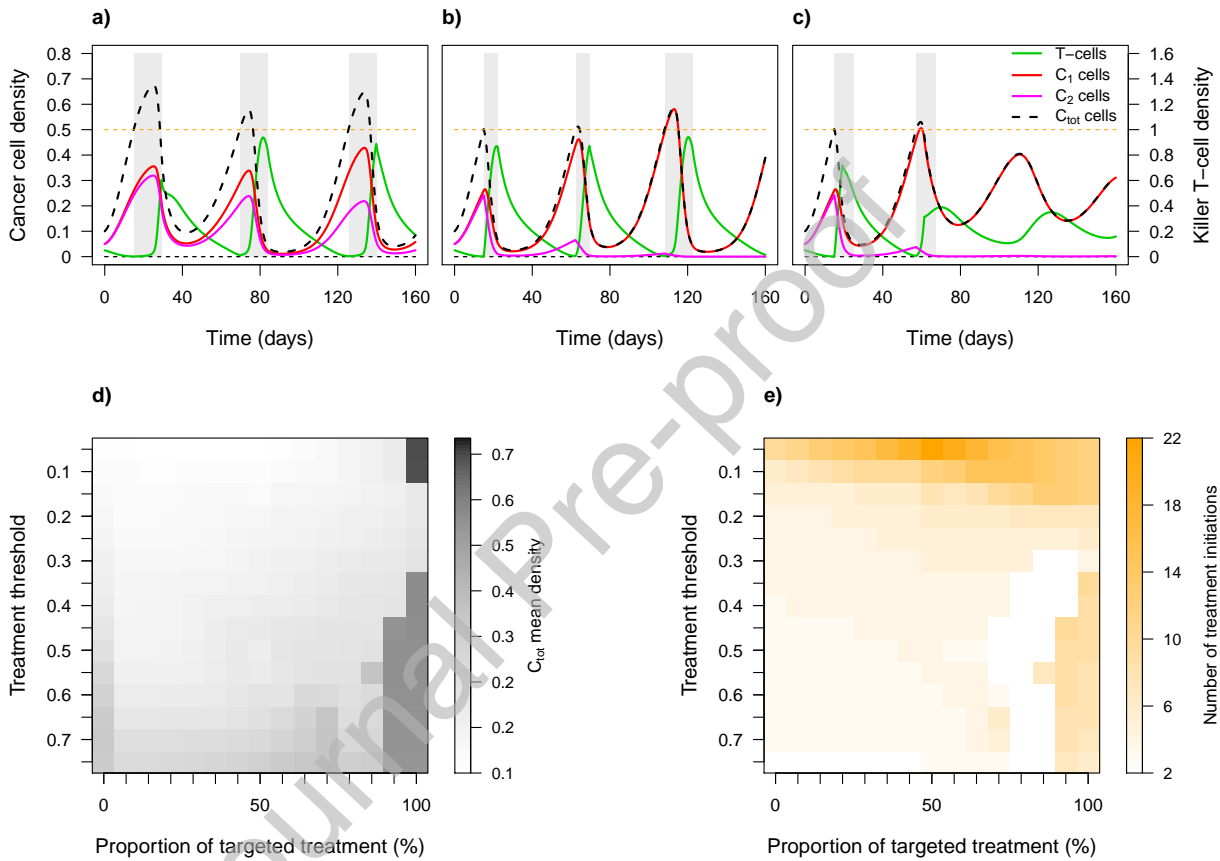
Figure 7: Combined effect of targeted and immunotherapy. a) Immunotherapy with period of 14 is initiated when the total cancer cell density goes over the treatment threshold of 0.4. b) Immunotherapy period of 7 days is given with simultaneous 7 days period of targeted treatment that is effective against the cancer cell subpopulation C_2. c) Targeted therapy period of 10 days combined with simultaneous immunotherapy period of 4 days. d) Total cancer cell population mean density when the treatment threshold and division of treatment durations is changed. The combined treatment time is fixed to 14 days, and hence the durations of targeted and immunotherapy can be calculated from the proportion of targeted therapy. For example proportion of 50% targeted treatment means 7 days of targeted treatment in combination with 7 days of simultaneous immunotherapy. e) The corresponding numbers of treatment initiations.
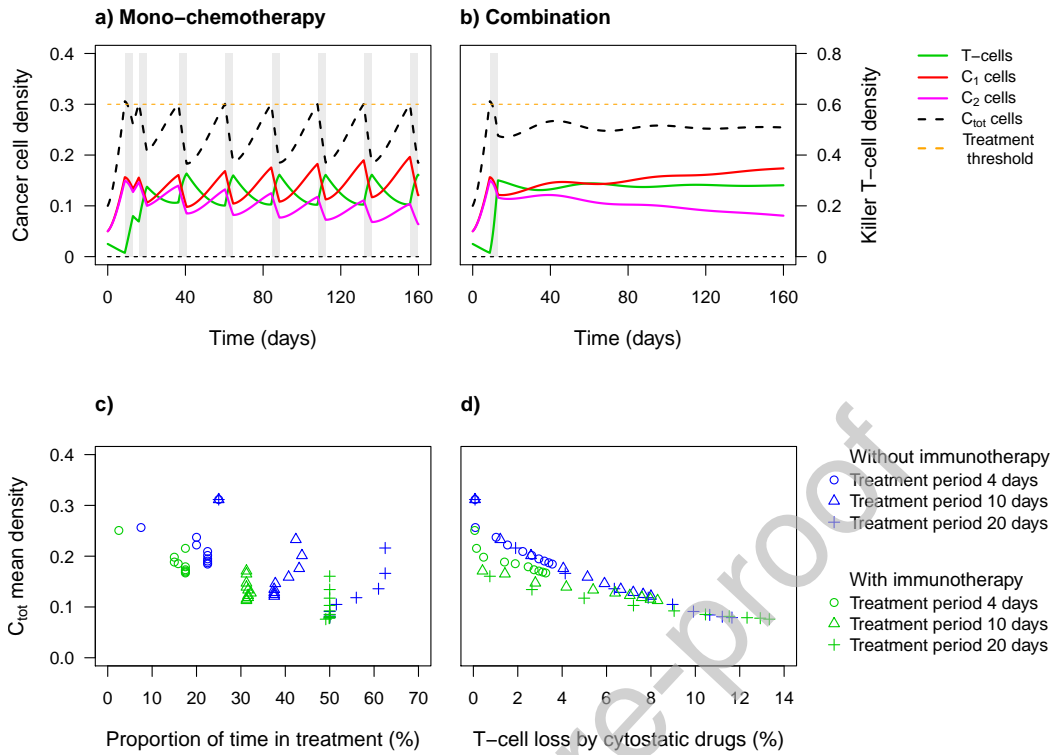
20

Figure 8: Combination effects of chemotherapy and immunotherapy. a) Mono-chemotherapy with a period of 4 days is initiated when the total cancer cell count exceeds 0.3. b) Chemotherapy in a combination with immunotherapy with the same duration of 4 days. c) The total cancer cell mean density drawn against proportion of time in treatment when the treatment period is 4, 10 or 20 days with and without immunotherapy. The concentration of cytostatic drug varies across the points marked with the same symbol. d) Side-effects caused by chemotherapy on T-cells in the corresponding cases.

3.6. Sensitivity analysis

To investigate how sensitive the results are to the changes in the model parameters, we perturbed the underlying biological parameter values that remained constant in the virtual melanoma patients (increased and decreased 25% from their values listed in Table 1). It was observed, generally, that increasing $\hat{R}$, K, γ or λ led to increases in the maximum cancer cell density, as expected, whereas decreasing these parameters reduced the maximum cancer cell density accordingly (Table 4). Similarly, increases in the resource competition between the cancer cell populations w reduced the maximum cancer cell density, and vice versa. Under treatment, these general conclusions remain the same. However, the cancer cell mean density did not behave similarly with and without treatment. As the cancer cell density increased faster, the T-cell density was affected as well, and accordingly the treatment succeeded more often with the treatment options that caused failure with the original parameter value. On the other hand, if the total cancer cell level decreased below the specified treatment threshold, the treatment was naturally not initiated at all leading to decreased killer T-cell mean density and increased cancer cell mean density. For example, the effect of changing $\hat{R}$ on total cancer cell mean density in the case study 2 (section 3.3) is shown in Supplementary Figure 9. The sensitivity analysis shows that increasing the killer T-cell self-regulation parameter δ reduced the killer T-cell levels, as expected, and decreasing δ had the opposite effect, with neither one changing the general conclusions made about the treatment efficacy. Since θ affects many interactions in the model (T-cell activation and interactions between cancer cells and T-cells), changing it had treatment sensitizing effects. Systematic sensitivity analyses are detailed in Supplementary section 8.
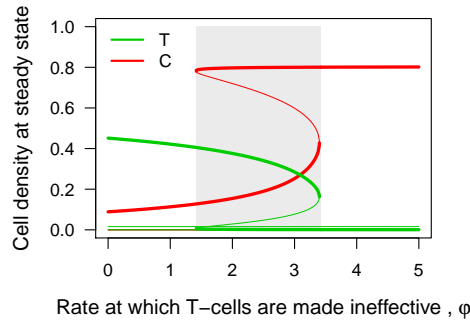
Figure 9: Steady states of cancer cells (C) and killer T-cells (T) as the value of φ is changed and other parameters are kept constant as in the case study 1. The grey bar denotes the range where two stable steady states exist.

Analysis of steady states was performed in the case study 1 with more parameters and larger change ranges (Supplementary section 8.1.1). It was observed, for instance, that when the rate at which cancer cells make active killer T-cells ineffective (φ) is between 1.40 and 3.42, two stable steady states exist (grey bar in Figure 9), and it is possible to move from one attractor to the other with carefully scheduled treatment (e.g., one used in Figure 3). In the case study 1, $\varphi = 3$, and the attractor is changed after single-shot immunotherapy (see Figure 3). However, when the rate is high ($3.42 \leq \varphi \leq 5$), only a single stable steady state exists with relatively high cancer cell density. In this case, the cancer cell density returns to that level even if it is temporarily decreased during treatment. When the rate is small ($0 \leq \varphi \leq 1.40$), only one stable steady state exists as well. However, the cancer cell density is already relatively low and depending of the treatment threshold value, the treatment might not be initiated at all. For all investigated parameters, it is important to identify, in which parameter value range there are more than one stable steady state (attractor can be changed with treatment), and, in the case of single stable steady state, if the cancer cell density is high (treatment is only temporary solution) or already relatively low (treatment might not be necessary). Steady states for cancer cells and T-cells were calculated with R-script grind.R (http://tbb.bio.uu.nl/rdb/grindR/grind.R).

As the dynamics of cancer and immune system are complex, it is not surprising that the outcome of treatment is sensitive to exact rates of interactions. Ideally, all parameters are patient-specific, and should be measured from individual patients. However, this is not yet realistic in clinical practice and parameter values estimated from cell lines or in general population have to be used. Individually, the most important parameters are the interactions between cancer cells and T-cells. For example, if the rate at which T-cells kill cancer cells (ξ_i) is too low (≤ 1.34 in the case study 1), only a single stable steady state exists and treatment can only temporarily decrease the cancer cell density (see Supplementary Figure 8k). Similarly, the infiltration of T-cells into the microenvironment of cancer depends on the individual's physiology. If T-cells cannot infiltrate the microenvironment of cancer ($\theta = 0$), the possible effect of treatment is only temporary since the only stable steady state for cancer density is relatively high. Additionally, the cancer cells might inhibit the immune response (e.g., CTLA4), leading to decreased or non-existent activation of killer T-cells ($m = 0$). The maximum rate of T-cell activation (m) should be high enough (≥ 0.45 in the case study 1) that a stable steady state with lower cancer cell density exists (see Supplementary Figure 8i). Luckily, there are therapies (e.g., anti-CTLA4), that may help patients with inhibited immune response (Chen and Mellman, 2013).

4. Discussion

We have developed a comprehensive model for the dynamics of active killer T-cells and their competition against distinct cancer cell populations under various treatment modalities. To our knowledge, this is the first

	Without treatment				With treatment			
Change	T mean dens.	T_{max}	C mean dens.	C_{max}	T mean dens.	T_{max}	C mean dens.	C_{max}
$\hat{R} \uparrow$	$+11\%$	0%	$+43\%$	$+42\%$	$+224\%$	$+79\%$	-1%	$+15\%$
$\hat{R} \downarrow$	0%	0%	-45%	-44%	-73%	-58%	$+20\%$	-20%
$K \uparrow$	$+1\%$	0%	$+4\%$	$+4\%$	$+6\%$	$+3\%$	0%	$+1\%$
$K \downarrow$	-2%	0%	-6%	-6%	-11%	-7%	$+4\%$	-2%
$\gamma \uparrow$	$+9\%$	0%	$+44\%$	$+42\%$	$+225\%$	$+78\%$	-1%	$+14\%$
$\gamma \downarrow$	$+5\%$	0%	-45%	-44%	-73%	-58%	$+20\%$	-19%
$\delta \uparrow$	0%	0%	0%	0%	-10%	-8%	$+6\%$	$+1\%$
$\delta \downarrow$	0%	0%	0%	0%	$+7\%$	$+6\%$	-7%	-1%
$\theta \uparrow$	-14%	0%	0%	0%	$+2\%$	$+9\%$	-9%	0%
$\theta \downarrow$	$+22\%$	0%	0%	0%	$+17\%$	-2%	$+18\%$	$+4\%$
$w \uparrow$	-3%	0%	-13%	-13%	-23%	-15%	$+10\%$	-4%
$w \downarrow$	$+4\%$	0%	$+14\%$	$+14\%$	$+45\%$	$+20\%$	-4%	$+4\%$
$\lambda \uparrow$	$+3\%$	0%	$+11\%$	$+11\%$	$+631\%$	$+173\%$	-9%	$+1\%$
$\lambda \downarrow$	-3%	0%	-14%	-14%	$+401\%$	$+107\%$	$+6\%$	-5%

Table 4: The change percentages of killer T-cell mean density, maximum T-cell density, cancer cell mean density and maximum cancer cell density on average over all case studies and treatment options. Parameter values are increased (↑) or decreased (↓) 25% from their value listed in Table 1. Only one parameter value is changed at a time, while others are kept constant. Mean dens. denotes mean density.

mathematical model that incorporates all the key aspects required for studying the individualized effects of anti-PD-1 immunotherapies in combination with targeted and chemotherapies, in terms of both therapeutic and side-effects. Importantly, rather than using the traditional approach that defines the cancer cell populations based on their genetic makeup alone, we consider also other, non-genetic differences that make the cell populations either sensitive or resistant to a therapy. Our model can be easily tailored to different scenarios, consisting of individual patients and treatment regimens. Here, we showed how the model provides insights into immunotherapy when comparing pre-set period treatment to more flexible threshold-based treatment initiation. It was noted that pre-set periods have to be chosen carefully in order to receive positive outcome. Interestingly, starting with tighter treatment schedule (shorter drug holidays) may enable a sparser treatment schedule later on. Additionally combination of targeted and immunotherapy was investigated, which results in a better treatment effect (cancer cell mean density) with fewer treatment initiations if used in suitable relation to each other. A stable disease might be also reached with few treatment initiations using combination therapy or targeted mono-therapy with carefully chosen treatment thresholds. Similar results were seen when using combination of chemotherapy and immunotherapy in comparison to chemotherapy alone. Combination results in smaller or equal level of cancer mean density and treatment times.

Systematic analysis of the effects of the various treatment choices was investigated through measures that capture the therapeutic benefit and toxic side-effects of the considered regimens. For example, tumor burden, measured as population mean of cancer cells, and time spend on treatment, both for immuno- and other therapies, quantify the efficacy of the treatment and the possible stress it causes to the patient and expenses to the health care operator, respectively. However, the eventual success of a treatment regimen is often determined by a subtle trade-off between the therapy-driven tumor burden reduction and toxic side-effects, as a function of the treatment intensity (so-called therapeutic window). Since there are individual differences in how patients experience both the therapy and its side-effects, the preferred treatment regimen that maximizes the tumor reduction might not be tolerated in clinical practice. Therefore, it is important to consider these different measures of treatment responses when deciding optimal regimens for a given patient. Previous model-based studies have also demonstrated the importance of high-resolution, dynamic monitoring of the cancer populations to achieve a given objective (e.g. adaptive treatment or cancer control) (Fassoni et al., 2019; Fischer et al., 2015; Khan et al., 2018; Komarova et al., 2014; Lai et al., 2019; Zhang et al., 2017).

In addition to the individual differences, the complexity of cancer and human biology poses challenges to the treatment response modelling. In the future work, it would be interesting to include, for example, the effect from disrupted angiogenesis (resistance to anti-angiogenic therapy (Bergers and Hanahan, 2008), evolution of angiogenic potential in cancer cells (Nagy and Armbruster, 2012)), adaptation to low level of resources, quiescent cells (trade-off of proliferation speed and adaptation to stressful conditions (Aktipis et al., 2013)), or delay in the response to immunotherapy. Furthermore, the emergence of new mutations or other molecular aberrations will be important to consider for modelling clonal evolution, since the relapse is often caused by new resistant clones that occur either due to cancer evolution or in response to chemotherapies (Gerlinger and Swanton, 2010; Kozłowska et al., 2018). In the present work, we considered two cancer subpopulations (sensitive and resistant), but the model can be extended to multiple dynamically-adapting populations, once the underlying rules of clonal evaluation are specified.

In the current model, it was assumed that cancer cells make active killer T-cells ineffective with PD-1/PD-L1 binding and that the ineffective T-cells exit the system without possibility to become effective. However, some drugs are able to cancel the PD-1 activation and render the ineffective killer T-cells effective again (Sakuishi et al., 2011). This re-activation effect could be considered as an additional component in the current model, as well as modelling different mechanisms of immunotherapies (e.g., CTLA4) or differing targeted therapies (e.g., those having direct positive or negative effect on T-cells, or those helping T-cells to enter into the microenvironment (Chen and Mellman, 2013)). Additionally, different combination treatment regimens could be considered, for example chemotherapy and immunotherapy given separately in sub-sequent time periods. Furthermore, the amount of T-cells and their functionality does not go hand in hand, meaning that higher amount of T-cells does not necessarily mean more efficacy against cancer,

24

which could be considered in further investigations. Similarly, adding various types of immune cells, including regulatory T-cells or natural killer cells, would more faithfully model the real immune-system component.

In order not to make it overly complicated, the current model lacks many aspects of cancer and immune response, some of which are mentioned above. Multiple parameters (e.g., inflow of resources, drug concentration) are thought as constants for simplicity, while in real patient these parameters change in time or over the disease progression. Even though adding more aspects into the model will make it more realistic, it also poses challenges to its analysis and estimation with limited data. Our aim in this work was therefore to model only those aspects we deem most important for the dynamic competition between active killer T-cells and cancer cell populations under the selected treatment modalities. To widen the potential applications of the model, one of our future aims is to make use of laboratory measurements in cancer cell line co-cultures, under selected treatment options, to fit the most critical model parameters with real-world measurements, and to evaluate the model qualitative behavior against that seen in the laboratory experiments. Eventually, with better estimated parameters, the model could be used to predict the effectiveness and consequences of various treatment choices as well the occurrence and timing of cancer relapse. We hope this will lead to more realistic set-up for tailoring treatment choices for individual cancer patients based on careful profiling of their primary tumor samples.

Authors' contributions

ASH implemented the model, made the analyses and produced the figures. ASH, TA and KP designed the study and wrote the manuscript. TA and KP supervised the work and conceived the study. SM and HK provided clinical expertise and critically reviewed the manuscript from medical perspective.

Acknowledgements

Funding

Declarations of interest

None.

References

Aguirre-Ghiso, J.A., 2007. Models, mechanisms and clinical evidence for cancer dormancy. Nature Reviews Cancer 7, 834–846. doi:10.1038/nrc2256.

Aktipis, C.A., Boddy, A.M., Gatenby, R.A., Brown, J.S., Maley, C.C., 2013. Life history trade-offs in cancer evolution. Nature Reviews Cancer 13, 883–892. doi:10.1038/nrc3606.

Bergers, G., Hanahan, D., 2008. Modes of resistance to anti-angiogenic therapy. Nature Reviews Cancer 8, 592–603. doi:10.1038/nrc2442.

Bhatia, S., Tykodi, S.S., Thompson, J.A., 2009. Treatment of metastatic melanoma: an overview. Oncology (Williston Park, N.Y.) 23, 488–96.

Bozic, I., Nowak, M.A., 2014. Timing and heterogeneity of mutations associated with drug resistance in metastatic cancers. Proceedings of the National Academy of Sciences 111, 15964–15968. doi:10.1073/pnas.1412075111.

Bozic, I., Reiter, J.G., Allen, B., Antal, T., Chatterjee, K., Shah, P., Moon, Y.S., Yaqubie, A., Kelly, N., Le, D.T., Lipson, E.J., Chapman, P.B., Diaz, L.A., Vogelstein, B., Nowak, M.A., 2013. Evolutionary dynamics of cancer in response to targeted combination therapy. eLife 2013, 1–16. doi:10.7554/eLife.00747.

Chen, D.S., Irving, B.A., Hodi, F.S., 2012. Molecular pathways: Next-generation immunotherapy-inhibiting programmed death-ligand 1 and programmed death-1. Clinical Cancer Research 18, 6580–6587. doi:10.1158/1078-0432.CCR-12-1362.

Chen, D.S., Mellman, I., 2013. Oncology Meets Immunology: The Cancer-Immunity Cycle. Immunity 39, 1–10. doi:10.1016/j.immuni.2013.07.012.

Dancey, A.L., Mahon, B.S., Rayatt, S.S., 2008. A review of diagnostic imaging in melanoma. Journal of Plastic, Reconstructive and Aesthetic Surgery 61, 1275–1283. URL: http://dx.doi.org/10.1016/j.bjps.2008.04.034, doi:10.1016/j.bjps.2008.04.034.

Disis, M.L., 2010. Immune regulation of cancer. Journal of Clinical Oncology 28, 4531–4538. doi:10.1200/JCO.2009.27.2146.

Dunn, G.P., Old, L.J., Schreiber, R.D., 2004. The immunobiology of cancer immunosurveillance and immunoediting. doi:10.1016/j.immuni.2004.07.017.

Fassoni, A.C., Roeder, I., Glauche, I., 2019. To Cure or Not to Cure : Consequences of Immunological Interactions in CML Treatment. Bulletin of Mathematical Biology doi:10.1007/s11538-019-00608-x.

Ferguson, T.A., Choi, J., Green, D.R., 2011. Armed response: How dying cells influence T-cell functions. Immunological Reviews 241, 77–88. doi:10.1111/j.1600-065X.2011.01006.x.

Fischer, A., Vázquez-García, I., Mustonen, V., 2015. The value of monitoring to control evolving populations. Proceedings of the National Academy of Sciences 112, 1007–1012. doi:10.1073/pnas.1409403112.

Fortin, P., Mackey, M.C., 1999. Periodic chronic myelogenous leukaemia: Spectral analysis of blood cell counts and aetiological implications. British Journal of Haematology 104, 336–345. doi:10.1046/j.1365-2141.1999.01168.x.

Garbe, C., Peris, K., Hauschild, A., Saiag, P., Middleton, M., Bastholt, L., Grob, J.J., Malvehy, J., Newton-Bishop, J., Stratigos, A.J., Pehamberger, H., Eggermont, A.M., 2016. Diagnosis and treatment of melanoma. European consensus-based interdisciplinary guideline - Update 2016. European Journal of Cancer 63, 201–217. doi:10.1016/j.ejca.2016.05.005.

Gauci, M.L., Lanoy, E., Champiat, S., Caramella, C., Ammari, S., Aspeslagh, S., Varga, A., Baldini, C., Bahleda, R., Gazzah, A., Michot, J.M., Postel-Vinay, S., Angevin, E., Ribrag, V., Hollebecque, A., Soria, J.C., Robert, C., Massard, C., Marabelle, A., 2019. Long-term survival in patients responding to anti-PD-1/PD-L1 therapy and disease outcome upon treatment discontinuation. Clinical Cancer Research 25, 946–956. doi:10.1158/1078-0432.CCR-18-0793.

Gerlinger, M., Swanton, C., 2010. How Darwinian models inform therapeutic failure initiated by clonal heterogeneity in cancer medicine. British Journal of Cancer 103, 1139–1143. doi:10.1038/sj.bjc.6605912.

Gesztelyi, R., Zsuga, J., Kemeny-Beke, A., Varga, B., Juhasz, B., Tosaki, A., 2012. The Hill equation and the origin of quantitative pharmacology. Archive for History of Exact Sciences 66, 427–438. doi:10.1007/s00407-012-0098-5.

Gillies, R.J., Verduzco, D., Gatenby, R.A., 2012. Evolutionary dynamics of carcinogenesis and why targeted therapy does not work. Nature Reviews Cancer 12, 487–493. doi:10.1038/nrc3298.

Glauche, I., Kuhn, M., Baldow, C., Schulze, P., Rothe, T., Liebscher, H., Roy, A., Wang, X., Roeder, I., 2018. Quantitative prediction of long-term molecular response in TKI-treated CML – Lessons from an imatinib versus dasatinib comparison. Scientific Reports 8, 1–13. doi:10.1038/s41598-018-29923-4.

Greaves, M., 2015. Evolutionary determinants of cancer. Cancer discovery 5, 806–20. doi:10.1158/2159-8290.CD-15-0439.

Huang, A.C., Orlowski, R.J., Xu, X., Mick, R., George, S.M., Yan, P.K., Manne, S., Kraya, A.A., Wubbenhorst, B., Dorfman, L., D'Andrea, K., Wenz, B.M., Liu, S., Chilukuri, L., Kozlov, A., Carberry, M., Giles, L., Kier, M.W., Quagliarello, F., McGettigan, S., Kreider, K., Annamalai, L., Zhao, Q., Mogg, R., Xu, W., Blumenschein, W.M., Yearley, J.H., Linette, G.P., Amaravadi, R.K., Schuchter, L.M., Herati, R.S., Bengsch, B., Nathanson, K.L., Farwell, M.D., Karakousis, G.C., Wherry, E.J., Mitchell, T.C., 2019. A single dose of neoadjuvant PD-1 blockade predicts clinical outcomes in resectable melanoma. Nature Medicine 25, 454–461. doi:10.1038/s41591-019-0357-y.

Keenan, T.E., Burke, K.P., Van Allen, E.M., 2019. Genomic correlates of response to immune checkpoint blockade. Nature Medicine 25, 389–402. doi:10.1038/s41591-019-0382-x.

Khan, K.H., Cunningham, D., Werner, B., Vlachogiannis, G., Spiteri, I., Heide, T., Mateos, J.F., Vatsiou, A., Lampis, A., Damavandi, M.D., Lote, H., Huntingford, I.S., Hedayat, S., Chau, I., Tunariu, N., Mentrasti, G., Trevisani, F., Rao, S., Anandappa, G., Watkins, D., Starling, N., Thomas, J., Peckitt, C., Khan, N., Rugge, M., Begum, R., Hezelova, B., Bryant, A., Jones, T., Proszek, P., Fassan, M., Hahne, J.C., Hubank, M., Braconi, C., Sottoriva, A., Valeri, N., 2018. Longitudinal liquid biopsy and mathematical modeling of clonal evolution forecast time to treatment failure in the prospect-c phase ii colorectal cancer clinical trial. Cancer Discovery 8. doi:10.1158/2159-8290.CD-17-0891.

Komarova, N.L., Burger, J.A., Wodarz, D., 2014. Evolution of ibrutinib resistance in chronic lymphocytic leukemia (CLL). Proceedings of the National Academy of Sciences 111, 13906–13911. doi:10.1073/pnas.1409362111.

Kozłowska, E., Färkkilä, A., Vallius, T., Carpén, O., Kemppainen, J., Grénman, S., Lehtonen, R., Hynninen, J., Hietanen, S., Hautaniemi, S., 2018. Mathematical modeling predicts response to chemotherapy and drug combinations in ovarian cancer. Cancer Research 78, 4036–4044. doi:10.1158/0008-5472.CAN-17-3746.

Lai, X., Geier, O.M., Fleischer, T., Garred, Ø., Borgen, E., Funke, S.W., Kumar, S., Rognes, M.E., Seierstad, T., Børresen-Dale, A.L., Kristensen, V.N., Engebråten, O., Köhn-Luque, A., Frigessi, A., 2019. Towards personalized computer simulation of breast cancer treatment : a multi-scale pharmacokinetic and pharmacodynamic model informed by multi-type patient data. Cancer research doi:10.1158/0008-5472.CAN-18-1804.

Laing, J.H., Wilson, G.D., Martindale, C.A., 2003. Proliferation rates in human malignant melanoma. Melanoma Research 13, 271–277. doi:10.1097/00008390-200306000-00008.

Lipson, E.J., Sharfman, W.H., Drake, C.G., Wollner, I., Taube, J.M., Anders, R.A., Xu, H., Yao, S., Pons, A., Chen, L., Pardoll, D.M., Brahmer, J.R., Topalian, S.L., 2013. Durable cancer regression off-treatment and effective reinduction therapy with an anti-PD-1 antibody. Clinical Cancer Research 19, 462–468. doi:10.1158/1078-0432.CCR-12-2625.

Louzoun, Y., Xue, C., Lesinski, G.B., Friedman, A., 2014. A mathematical model for pancreatic cancer growth and treatments. Journal of Theoretical Biology 351, 74–82. doi:10.1016/j.jtbi.2014.02.028.

Malhotra, V., Perry, M.C., 2003. Classical chemotherapy: mechanisms, toxicities and the therapeutic window. Cancer biology & therapy 2, 4–6. doi:10.4161/cbt.199.

Maverakis, E., Cornelius, L.A., Bowen, G.M., Phan, T., Patel, F.B., Fitzmaurice, S., He, Y., Burrall, B., Duong, C., Kloxin, A.M., Sultani, H., Wilken, R., Martinez, S.R., Patel, F., 2015. Metastatic melanoma – A review of current and future treatment options. Acta Dermato-Venereologica 95, 516–524. doi:10.2340/00015555-2035.

Michor, F., Beal, K., 2015. Improving Cancer Treatment via Mathematical Modeling: Surmounting the Challenges Is Worth the Effort. Cell 163, 1059–1063. doi:10.1016/j.cell.2015.11.002.

Motz, G.T., Coukos, G., 2013. Deciphering and Reversing Tumor Immune Suppression. Immunity 39, 61–73. doi:10.1016/j.immuni.2013.07.005.

Nagy, J.D., Armbruster, D., 2012. Evolution of uncontrolled proliferation and the angiogenic switch in cancer. Mathematical Biosciences and Engineering 9, 843–876. doi:10.3934/mbe.2012.9.843.

O'Donnell, J.S., Teng, M.W., Smyth, M.J., 2019. Cancer immunoediting and resistance to T cell-based immunotherapy. Nature Reviews Clinical Oncology 16, 151–167. doi:10.1038/s41571-018-0142-8.

Ossowski, L., Aguirre-Ghiso, J.A., 2010. Dormancy of metastatic melanoma. Pigment Cell and Melanoma Research 23, 41–56. doi:10.1111/j.1755-148X.2009.00647.x.

Pardoll, D.M., 2012. The blockade of immune checkpoints in cancer immunotherapy. Nature Reviews Cancer 12, 252–264. doi:10.1038/nrc3239.

Robert, C., 2018. Is earlier better for melanoma checkpoint blockade? Nature Medicine 24, 1645–1648. doi:10.1038/s41591-018-0250-0.

Robert, C., Long, G.V., Brady, B., Dutriaux, C., Maio, M., Mortier, L., Hassel, J.C., Rutkowski, P., McNeil, C., Kalinka-Warzocha, E., Savage, K.J., Hernberg, M.M., Lebbé, C., Charles, J., Mihalcioiu, C., Chiarion-Sileni, V., Mauch, C., Cognetti, F., Arance, A., Schmidt, H., Schadendorf, D., Gogas, H., Lundgren-Eriksson, L., Horak, C., Sharkey, B., Waxman, I.M., Atkinson, V., Ascierto, P.A., 2015. Nivolumab in previously untreated melanoma without BRAF mutation. New England Journal of Medicine 372, 320–330. doi:10.1056/NEJMoa1412082.

Sakuishi, K., Apetoh, L., Sullivan, J.M., Blazar, B.R., Kuchroo, V.K., Anderson, A.C., 2011. Targeting Tim-3 and PD-1 pathways to reverse T cell exhaustion and restore anti-tumor immunity. The Journal of Experimental Medicine 208, 2187–2194. doi:10.1084/jem.201006432011512c.

Schreiber, R.D., Old, L.J., Smyth, M.J., 2011. Cancer immunoediting: Integrating immunity's roles in cancer suppression and promotion. Science 331, 1565–1570. doi:10.1126/science.1203486.

Senft, D., Ronai, Z.A., 2016. Immunogenic, cellular, and angiogenic drivers of tumor dormancy-a melanoma view. Pigment Cell and Melanoma Research 29, 27–42. doi:10.1111/pcmr.12432.

Smith, H.L., Waltman, P.E., 1995. The theory of the chemostat : dynamics of microbial competition. Cambridge University Press.

Stark, J., Chan, C., George, A.J., 2007. Oscillations in the immune system. Immunological Reviews 216, 213–231. doi:10.1111/j.1600-065X.2007.00501.x.

Tannock, I.F., 1968. The relation between cell proliferation and the vascular system in a transplanted mouse mammary tumour. British Journal of Cancer 22, 258–273. doi:10.1038/bjc.1968.34.

Tokuyasu, H., Ishikawa, S., Sakai, H., Ikeuchi, T., Miura, H., 2019. Single pembrolizumab treatment causing profound durable response in a patient with pulmonary pleomorphic carcinoma. Respiratory Medicine Case Reports 28, 26–30. doi:10.1016/j.rmcr.2019.100879.

Topalian, S.L., Sznol, M., McDermott, D.F., Kluger, H.M., Carvajal, R.D., Sharfman, W.H., Brahmer, J.R., Lawrence, D.P., Atkins, M.B., Powderly, J.D., Leming, P.D., Lipson, E.J., Puzanov, I., Smith, D.C., Taube, J.M., Wigginton, J.M., Kollia, G.D., Gupta, A., Pardoll, D.M., Sosman, J.A., Hodi, F.S., 2014. Survival, durable tumor remission, and long-term safety in patients with advanced melanoma receiving nivolumab. Journal of Clinical Oncology 32, 1020–1030. doi:10.1200/JCO.2013.53.0105.

Tóth, P., Érdi, J., 1989. Mathematical Models of Chemical Reactions: Theory and Applications of Deterministic and Stochastic Models. Manchester University Press.

Tufto, I., Rofstad, E.K., 1998. Interstitial Fluid Pressure, Fraction of Necrotic Tumor Tissue, and Tumor Cell Density in Human Melanoma Xenografts. Acta Oncologica 37, 291–297. URL: http://www.tandfonline.com/doi/full/10.1080/028418698429603, doi:10.1080/028418698429603.

Wolner, Z.J., Marghoob, A.A., Pulitzer, M.P., Postow, M.A., Marchetti, M.A., 2018. A case report of disappearing pigmented skin lesions associated with pembrolizumab treatment for metastatic melanoma. British Journal of Dermatology 178, 265–269. doi:10.1111/bjd.15354.

Zhang, J., Cunningham, J.J., Brown, J.S., Gatenby, R.A., 2017. Integrating evolutionary dynamics into treatment of metastatic castrate-resistant prostate cancer. Nature Communications 8, 1–10. doi:10.1038/s41467-017-01968-5.

Zhao, B., Hemann, M.T., Lauffenburger, D.A., 2016. Modeling tumor clonal evolution for drug combinations design. Trends in Cancer 2, 144–158. doi:10.1016/j.trecan.2016.02.001.

Zhou, J., Wang, G., Chen, Y., Wang, H., Hua, Y., Cai, Z., 2019. Immunogenic cell death in cancer therapy: Present and emerging inducers. Journal of Cellular and Molecular Medicine 23, 4854–4865. doi:10.1111/jcmm.14356.

Modelling of killer T-cell and cancer cell subpopulation dynamics under immuno- and chemotherapies

Anni S. Halkola, Kalle Parvinen, Henna Kasanen, Satu Mustjoki, Tero Aittokallio

CRediT author statement:

Anni S. Halkola: Methodology, Software, Formal analysis, Writing – Original Draft, Writing – Review & Editing, Visualization.

Kalle Parvinen: Conceptualization, Methodology, Writing – Original Draft, Writing – Review & Editing, Supervision.

Henna Kasanen: Writing – Review & Editing.

Satu Mustjoki: Writing – Original Draft, Writing – Review & Editing.

Tero Aittokallio: Conceptualization, Methodology, Writing – Original Draft, Writing – Review & Editing, Supervision, Project administration.